Hindawi
Journal of Nanotechnology
Volume 2017, Article ID 5219850, 8 pages
https://doi.org/10.1155/2017/5219850

*Research Article*

# Sol-Gel Syntheses of Zinc Oxide and Hydrogenated Zinc Oxide (ZnO:H) Phases

**Joshua Lelesi Konne and Bright Obum Christopher**

*Department of Chemistry, Rivers State University of Science and Technology, Nkpolu, Oroworukwo, Port Harcourt, Nigeria*

Correspondence should be addressed to Joshua Lelesi Konne; konne.joshua@ust.edu.ng

Received 26 June 2016; Revised 29 November 2016; Accepted 5 December 2016; Published 5 January 2017

Academic Editor: Marco Rossi



ZnO synthesized by chemical precipitation with varying starch concentrations (0.00, 0.01, 0.02, 0.05, 0.10, 0.15, and 0.20%) as stabilizing agent was used in making ZnO:H when placed in a glass tube under mild heat and hydrogen ($H_2$) gas flow for 2 mins. Observations showed that the sample colour changed from white to light brown and finally to dark brown during the process particularly for the ZnO-starch samples. XRD data of ZnO (0.02%) and ZnO:H (0.02%) showed ZnO as the major phase with $Zn(OH)_2$ impurity phase and a new ZnO:H peak at $2\theta$, 29.60° for ZnO and ZnO:H, respectively. The estimated particle sizes determined from XRD were 47 and 30 nm, respectively. The SEM of the 0.02% ZnO appeared more microporous and needle-like than those of 0.01%, while the EDX of both confirmed Zn and O as the main components. Different conductivities of 30.90 and 27.50 $\mu$S/cm were obtained for ZnO and ZnO:H samples in ethanol, respectively. Also, the UV-Vis absorption for both showed n-type and p-type material absorption bands at 310 $cm^{-1}$, while the intensities of all the characteristic ZnO IR bands at 430–552 (ZnO vibrations) and 1500–1640 $cm^{-1}$ (Zn-O stretching) increased for the corresponding ZnO:H samples.

## 1. Introduction

The compositions of Rock-Salt structures of some 3D-metal monoxides (MOs) like ZnO among others are mostly nonstoichiometric with defects and vacancies on either their cationic or anionic sites. These inherent variable compositions influence the electrical, mechanical, spectral, optical, magnetic, catalytic, antimicrobial, and even metallic properties of the MOs [1]. Hence MOs like ZnO find applications such as light diodes, transparent conductors, photocatalysts, photoprinting, solar cells, lasers, sensors, body powder, sunscreen and medicated creams, UV resistant coatings, capacitors, and varistor-electronic devices [2–4].

ZnO has a Wurtzite structure that exists in two phases as $Zn_{1-x}O$ or $ZnO_{1-x}$ depending on whether it is zinc deficient or zinc rich [1]. The two phases occur naturally during synthesis and are referred to as "native defects." While the zinc deficient phase is a strong electron acceptor, the oxygen deficient phase is a strong donor. In the donor form ($ZnO_{1-x}$), ZnO exhibits strong n-type semiconductivity in which electrical conductivity decreases due to withdrawal of electrons from the conduction band. Oxygen deficient phase has been attributed to the presence of commonly associated impurities such as hydrogen on the oxygen sites [5–7]. ZnO with n-type conductivity finds application for use in transparent solar cell conductors and displays and as bilayer for low-cost thin film electronics [8, 9].

The morphological control over crystallization of ZnO from nitrate salt and sodium hydroxide precursors has been found to be route, pH, temperature, and concentration dependent [2, 4]. Therefore ZnO has been synthesized by microemulsion [3], paper [10], hydrothermal [11] and mechanochemical decomposition [12], microwave-assisted [13], ionic-template [14], solvothermal [15], and pulsed Laser deposition [16], sol-gel (using zinc acetate, folic acid, and starch), and so forth for various applications [17–19]. Sol-gel technique is cheap and easy and produces purer high surface materials amongst others. However, the applications of these techniques including sol-gel in the production of intentionally synthesized hydrogenated zinc oxide nanoparticles (ZnO:H) phases have not been widely reported.

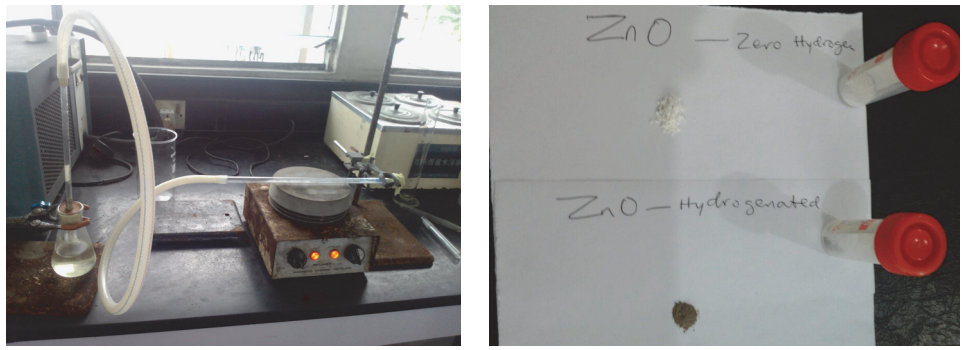


(a) (b)

Figure 1: (a) Hydrogenation of ZnO heated at 55°C using Mg ribbon dissolved in 6 M HCl and (b) labelled samples before and after hydrogenation.

Theoretical ab initio simulations have shown that hydrogen ($H^+$) ion substitutes oxygen vacancy forming a fourfold coordination with Zn atoms in hydrogenated ZnO, while Zn vacancy (which results in p-type conductivity) is substituted by two hydrogen atoms [6, 20]. Thus, a well-hydrogenated ZnO phase should have some structural changes (due to lattice adjustments for H insertion) that would affect Zn-O vibrations, UV absorption, and electrical conductivity [21–23]. Therefore, the adoption of a suitable synthetic strategy for ZnO:H could produce the desired control over n-type conductivity in ZnO. However, the available studies have not demonstrated such structural changes due to H insertion in hydrogenated ZnO phase using XRD. This report presents an adaptable approach to the sol-gel synthesis of hydrogenated ZnO nanoparticles (ZnO:H), UV-Vis study, X-ray diffraction, electrical conductivity analyses, and Infrared spectroscopic studies of both phases with varying particle sizes.

## 2. Experimental

*2.1. Synthesis of ZnO Nanoparticles.* Zinc oxide nanoparticles were synthesized by a modified wet chemical method involving the precipitation of zinc hydroxide, $Zn(OH)_2$, from the reaction of 0.1 mol zinc nitrate and 0.2 mol sodium hydroxide solutions followed by overnight drying of the precipitates at 80°C to form ZnO [19]. Varying masses of starch (0.01, 0.02, 0.05, 0.10, 0.15, and 0.20 g) were weighed and dissolved in 100 mL of deionized water to give the different % (w/v) concentrations. These solutions were boiled at 100°C, cooled, and used for the dissolution of precursors before reaction. Modifications to previous report [19] included direct boiling of starch solution (not microwaving), separation by decantation and filtration (not centrifuging), and use of boiled starch solutions for dissolution of precursors.

*2.2. Synthesis of ZnO:H Nanoparticles.* The generation of hydrogen ($H_2$) gas was achieved by the reaction of 10 pieces of Mg ribbon dissolved in 50 mL of 6 M HCl in a conical flask. The liberated hydrogen was passed over ZnO nanoparticles under mild heat (55°C) in a glass tube well clamped slightly above a heating mantle surface for 3 mins. The hydrogenation process was repeated thrice for one of 0.02% sample in order to investigate the effect of higher H-concentration. The setup for the process is shown in Figure 1(a). The colour of the ZnO nanoparticles changed from white to brown and finally to dark brown or black for the starch coated samples (Figure 1(b)). However, no visible change was observed for the control sample without starch (0%). The samples over which hydrogen gas was passed were tagged as $ZnO:H_{(a)}$ and $ZnO:H_{(b)}$ (hydrogenated process repeated thrice) samples, respectively.

*2.3. Characterization.* The X-ray diffraction (XRD) analyses of samples of 0.02% starch ($ZnO:H_{(a\&b)}$ and ZnO) were carried out on a GBC Enhanced Mini-Material Analyzer. The samples were ground into fine (homogeneous) powder, pelletized, and loaded on a silicon sample holder. Pelletizing was done in order to enhance smooth sample surface necessary for low noise output. The $2\theta$ angle range of 10–60°C within which major reflections of ZnO appear was selected with a step size of 0.05. Similarly, the conductivities of two samples ZnO and $ZnO:H_{(a)}$ dispersed in 10 mL ethanol were carried out with an Extech D0700 Conductivity Instrument. The same samples were used for a UV-Vis scan between 300 and 500 nm on a 2500 LaboMed spectrophotometer. The SEM samples were prepared by placing a little of the samples on carbon sticky pads. These were placed on labeled aluminum stubs prior to analysis on an SEM model ASPEX 3020 equipped with an Oxford EDX detector. The two starched samples first used for SEM and EDX analyses were those of the 0.01 and 0.02% ZnO samples only due to cost. Later, the SEM and energy dispersive spectroscopy (EDS) of both 0.02% (ZnO and $ZnO:H_{(b)}$), respectively, were also carried out in order to investigate possible impact of H insertion on the ZnO microstructures. Samples for FT-IR were ground with KBr and pelletized into circular discs for analysis on a PerkinElmer Spectrum 10.4.3 Infrared spectrophotometer. Each disc was placed in a sample holder positioned in the path

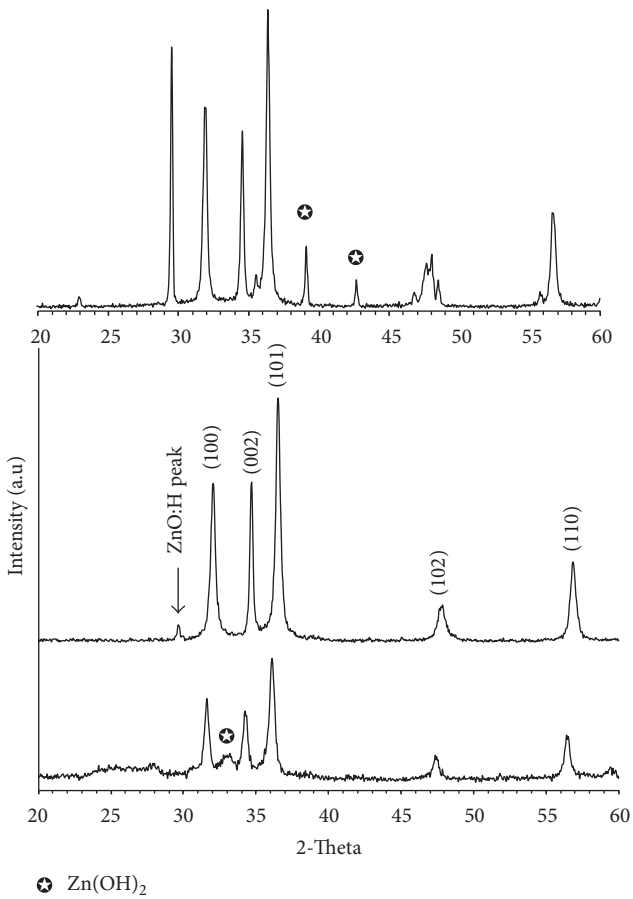


Figure 2: XRD patterns of 0.02% starch-mediated (ZnO-bottom, $ZnO:H_{(a)}$-middle, and $ZnO:H_{(b)}$-top) samples, respectively.

of Infrared radiation operating at a selected wavelength range of 350–4000 nm before the analysis on a read out computer.

## 3. Results and Discussion

*3.1. XRD, Conductivity, and SEM Characterizations.* The XRD patterns of the ZnO (bottom) and $ZnO:H_{(a\&b)}$ (top) plots for the 0.02% starch-mediated (ZnO and ZnO:H) samples, respectively, are shown in Figure 2. The major reflections of the samples were indexed to a hexagonal synthetic zincite of the space group, P63mc (186), using the Joint Committee on Powder Diffraction Standards (JCPDS) card number 00-005-0664 [24]. *c*-axis (002) was calculated as 0.520 nm and this matched with the reference card value of 0.5205 nm.

However, the ZnO and $ZnO:H_{(b)}$ samples showed reflections of minor $Zn(OH)_2$ impurity phase at $2\theta$, 33.20 (ZnO), 39.10 and 42.65° ($ZnO:H_{(b)}$), respectively, indexed to JCPDS card 38–385 [4], while both $ZnO:H_{(a)}$ and $ZnO:H_{(b)}$ showed the emergence of a new peak due to ZnO hydrogen bonded (ZnO:H) phases at $2\theta$, 29.60°, respectively. The enhancement of the peak assigned to ZnO:H as shown by the second sample ($ZnO:H_{(b)}$) where the hydrogenation process was repeated thrice (top image of Figure 2) confirmed the peak position. Moreover, the intermediate product, ($Zn(OH)_2$) does not reflect at such angle. Particle size estimations were evaluated from Scherrer's formula (see (1)) below:

$$\left[d = \frac{k\lambda}{\beta \cos\theta}\right], \tag{1}$$

where $d$ is mean particle diameter (size), $\lambda$ is Cu K$\alpha$1 radiation = 0.154 nm, $\beta$ is Full Width at Half Maximum (FWHM) (in radians), and $\theta$ is half of $2\theta$ angle (radians), respectively. The particle sizes estimated for the three samples were 47 (ZnO), 37 ($ZnO:H_{(b)}$), and 30 nm ($ZnO:H_{(a)}$) samples, respectively.

The difference in particle sizes of ZnO and $ZnO:H_{(a\&b)}$ samples could be attributed to hydrogen replacement of O atom in the 0.02% starch-mediated ZnO since the same sample (size) was used for $ZnO:H_{(a\&b)}$ synthesis and as such no change should have occurred except from H replacement of O atom in a fourfold coordinated position [6, 21]. In addition, the presence of $Zn(OH)_2$ impurities could also be a factor as observed for the size variation between $ZnO:H_{(a)}$ and $ZnO:H_{(b)}$. Hydrogen doping which causes reduced conductivity in ZnO was also found to be responsible for the different conductivities of 30.90 and 27.50 $\mu$S/cm obtained for ZnO and $ZnO:H_{(a)}$ samples, respectively, in ethanol. The conductivity of the ethanol used was 8.41 $\mu$S/cm.

Furthermore, higher $d$-spacing was also obtained for ZnO compared to those of ZnO:H for the same peak positions. For instance, $d$-spacing of ZnO for (100) peak was 2.829, while those of $ZnO:H_{(a)}$ and $ZnO:H_{(b)}$ were 2.791 and 2.803, respectively, for the same peak position. Table 1 of the supplementary data sheet in Supplementary Material available online at https://doi.org/10.1155/2017/5219850 contained $d$-spacing of major peaks of the samples. These narrow shifts in peak positions ($d$-spacings) could be due to strain effects from inhomogeneity caused by H insertion. However, small changes in lattice parameters would only be observed in the case of uniform dilatation (equally strained polycrystallites) like those of $ZnO:H_{(b)}$ with higher hydrogen concentration compared to $ZnO:H_{(a)}$ [25].

The same starch solution (gel) was used for all three samples and this enhanced homogeneous nucleation of $Zn(OH)_2$ clusters and subsequent crystal growth of zinc oxide nanoparticles during the drying process. This effect is reflected in similar broad peaks and backgrounds observed in the XRD patterns of all three samples (Figure 2). The change in colour of the hydrogenated starch-mediated samples from white to brown and finally dark brown as shown in Figure 1 would be due to the presence of oxygen atoms on starch molecules in addition to those provided by ZnO groups compared to non-starch-mediated ZnO samples. The estimated particle size of ZnO obtained was slightly lower than ~50 nm reported for similar starch-mediated method with 0.1% starch [19].

The SEM images of two (0.01 and 0.02% starch-mediated) samples showed morphological differences of the synthesized ZnO nanoparticles as shown in Figures 3(a) and 3(b), respectively. Similar controls of crystal sizes with changing starch concentration have been reported previously [26]. The image in Figure 3(a) shows polycrystallite clusters of varying sizes in the form of porous agglomerates, while a more porous fiber-like network was observed in Figure 3(b) (0.02%

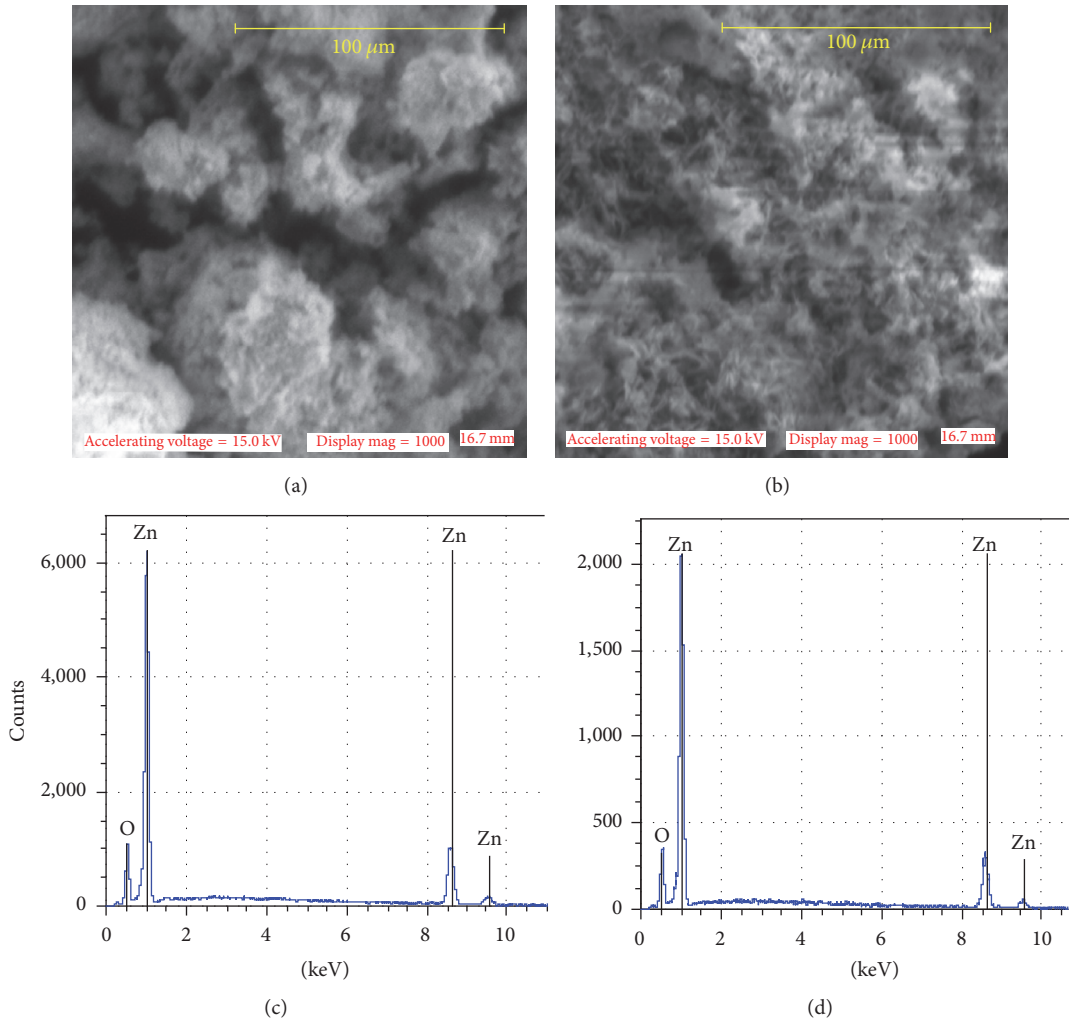


Figure 3: (a-b) SEM micrographs and (c-d) EDX spectra of 0.01% and 0.02% starch-mediated ZnO samples, respectively.

starch-mediated sample). The EDX spectra of both samples confirmed the presence of zinc and oxygen only in the two samples as shown in Figures 3(c) and 3(d), respectively.

Similarly, the SEM micrographs of the 0.02% starch ZnO at both higher and lower magnifications (Figures 4(a) and 4(b)) and those of ZnO:$H_{(b)}$ (Figures 4(c) and 4(d)) at similar magnifications are shown in Figure 4. ZnO:$H_{(b)}$ was selected for SEM analysis because of its higher hydrogen content than ZnO:$H_{(a)}$. ZnO at higher magnification with scale bar of 200 nm (Figure 4(a)) showed aggregates of thick-joint polycrystallites separated by pores, while the lower magnification (with 500 nm scale bar) showed a more compact microporous polycrystallite structure (Figure 4(b)). The higher magnified SEM micrographs (scale bar of 100 nm) of ZnO:$H_{(b)}$ in Figure 4(c) showed smaller grains of joint polycrystallites on top of larger ball-like structured materials with wider pores. The smaller crystallites could be the hydrogenated zinc oxide polycrystallites. However, at lower magnification with 500 nm scale bar (Figure 4(c)), an orderly etched monophasic surface was observed. The EDS of both samples appear on Figures 4(a) and 4(d) for ZnO and ZnO:$H_{(b)}$ samples, respectively. They showed Zn as the major components of both samples with ZnO:$H_{(b)}$ having lower Zn content of 54.42% compared to 56.68% of ZnO. Other elements (impurities) found on both EDS were Si, Mn, Fe, Ti, and Ca.

*3.2. UV-Vis and IR Characterizations.* A scan of the ZnO:$H_{(a)}$ sample in ethanol from 500 to 300 nm showed a strong excitonic absorption peak in the UV region at 310 nm corresponding to electron transition (withdrawal) from the conduction band of n-type (that is anion-deficient) $ZnO_{1-x}$ to the valence band. See Figure 5 for the UV-Vis absorption spectra of ZnO and ZnO:H, respectively.

The 310 nm band of excitation corresponds to an optical band gap of 3.99 eV above 3.7 eV reported in literature [3]. Despite other weaker excitonic absorptions at 340 nm (3.635 eV) and 450 nm (2.75 eV) probably due to inelastic scattering of charge by interacting phonons as the time progressed, the band at 310 nm was significant as it had a corresponding strong absorption by the ZnO (anionic rich) sample [2, 3, 12]. However, both samples had similar excitonic absorption at 450 nm. The observed differences in optical

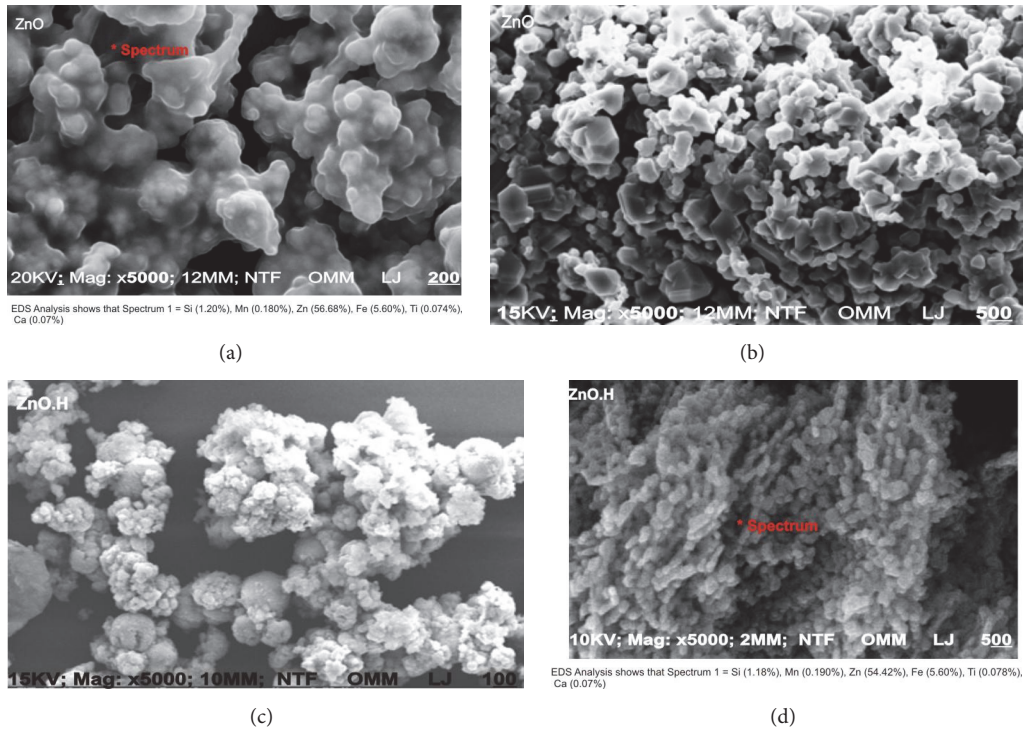


Figure 4: SEM micrographs of 0.02% starch (a-b) ZnO and (c-d) ZnO:$H_{(2)}$, respectively, with their EDS on (a) and (d), respectively.

behavior of the two samples in the UV region confirmed the structural changes due to H insertion. Hence, further studies were carried out on the 0, 0.05, and 0.15% starch-mediated ZnO and ZnO:$H_{(a)}$ samples, respectively, using the FT-IR spectroscopy in order to observe H insertion effect on the Zn-O bonds.

The results (spectra) of the FT-IR analysis of the samples are shown in Figures 6(a)–6(f). Infrared finger print region of most metal oxides occurs below 1000 $cm^{-1}$ and the characteristic Zn-O vibration bands (430–560 $cm^{-1}$) also lie in this region [10]. It was observed that the ZnO sample bands within these region became broadened with intense blue shift in their corresponding ZnO:H sample bands. For example, ZnO band (0%) at 552 $cm^{-1}$ shifted to 515 $cm^{-1}$ with a shoulder at 533 $cm^{-1}$ for its corresponding ZnO:H (0%) sample (Figures 6(a) and 6(b)).

Similar observations were made for Zn-O stretching bands at 1500–1640 $cm^{-1}$ [3] (Figures 6(a), 6(c), and 6(e)). However, with the H replacement of some O atoms, the Zn-O stretching vibrations merged into single but intense Zn-O-H stretching at 1633–1638 $cm^{-1}$ for all corresponding ZnO:H samples (Figures 6(b), 6(d), and 6(f)). This led to the disappearance of all peaks around 1500 $cm^{-1}$ in the ZnO:H samples. Thus all the ZnO:H (0, 0.05, and 0.15% starch-mediated) samples showed fewer bands due to the merged peaks (Figures 6(b), 6(d), and 6(f)). The crystallinity of the samples decreased with the addition of starch such that seven bands were lost between 0% and 0.05% of added starch

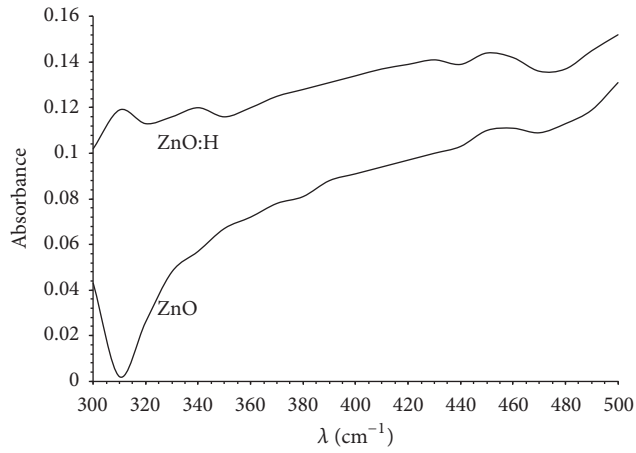


Figure 5: UV-Vis absorption spectra of ZnO and ZnO:H as a function of wavelength.

concentration. Further decrease was observed with the addition of hydrogen. The FT-IR bands of ZnO and ZnO:H are also contained in Table 2 of the supplementary information data sheet. Broad bands at 2000–3444 and 1114 $cm^{-1}$ (0%-ZnO:H) were assigned to O-H stretching and deformation, respectively, from adsorbed moisture on sample surface due to preparation in air [3]. Similar adsorbed free $CO_2$ from the air might be responsible for the band at 1384 $cm^{-1}$ present in all the samples including the control (0%).

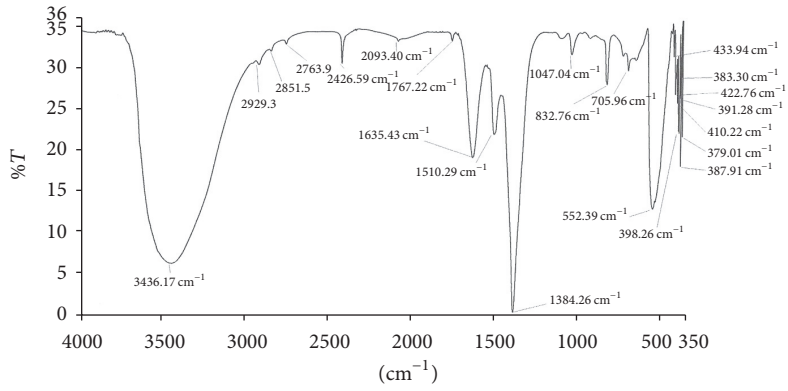


(a)

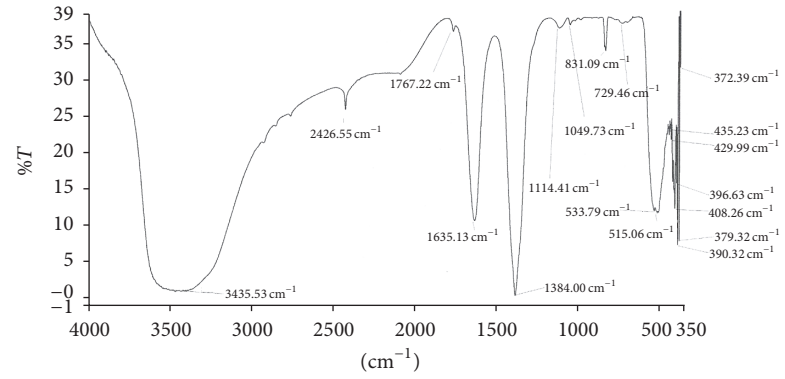


(b)

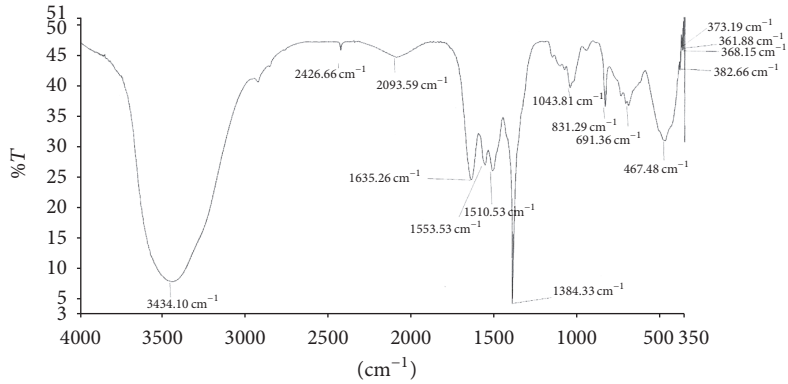


(c)

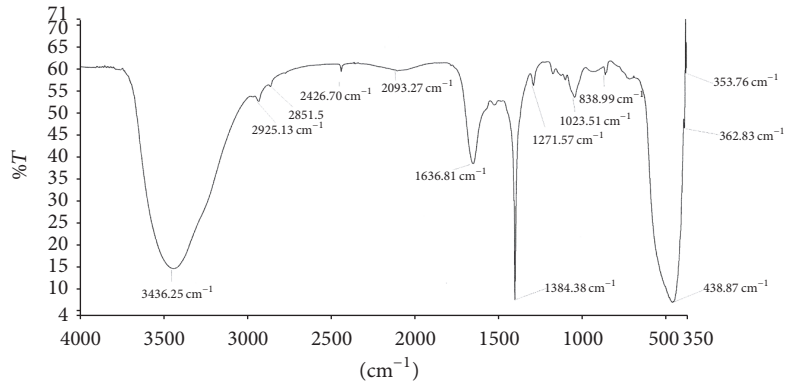


(d)

Figure 6: Continued.

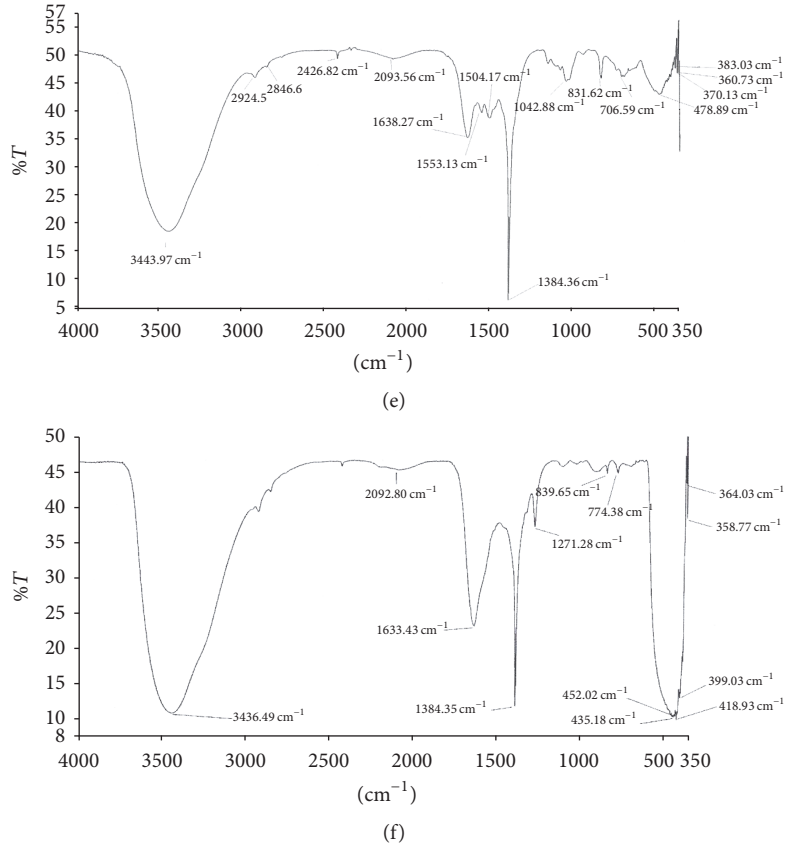


Figure 6: (a–f) FT-IR of ZnO and their corresponding ZnO:H samples at 0, 0.05, and 0.15% starch content of precursor solutions. (a) FT-IR of zinc oxide; ZnO synthesized using precursors in deionized water only, 0% starch (control). (b) FT-IR of hydrogenated zinc oxide; ZnO:H synthesized from precursors in deionized water only, 0% starch. (c) FT-IR of zinc oxide; ZnO synthesized using precursors in 0.05% starch solution. (d) FT-IR of hydrogenated zinc oxide; ZnO:H synthesized from precursors in 0.05% starch solution. (e) FT-IR of zinc oxide; ZnO synthesized using precursors in 0.15% starch solution. (f) FT-IR of hydrogenated zinc oxide; ZnO:H synthesized from precursors in 0.15% starch solution.

## 4. Conclusion

The sol-gel synthesis of ZnO and ZnO:H phases via a simple adaptable technique has been reported. The XRD results of both samples showed reflections that were indexed to standard ZnO pattern. However, the emergence of a new peak due to H insertion into the ZnO lattice was observed at $2\theta$, 29.60° for ZnO:$H_{(a)}$, and confirmed with intense peak from a more hydrogenated ZnO:$H_{(b)}$. Lower conductivity value of 27.50 $\mu$S/cm as well as the estimated particle size of 30 nm was recorded for ZnO:$H_{(a)}$ compared to 30.90 $\mu$S/cm and 47 nm for the ZnO samples, respectively. Evidence of H insertion in ZnO:$H_{(a)}$ samples was supported by the distinct excitonic electronic transition occurring concomitantly with strong absorption by ZnO samples at 310 nm in the UV region. The SEM of the 0.02% ZnO appeared more microporous and fiber-like than those of 0.01% starch-mediated samples, indicating that control over particle size was achieved *via* varying starch concentration, while the EDX confirmed Zn and O as the main components of the two samples. Higher magnification SEM of 0.02% ZnO:$H_{(b)}$ showed the presence of smaller grained polycrystallites surrounding larger ball-like polycrystallites indicating the biphasic microstructures due to H insertion. FT-IR results showed possible decrease in crystallinity (loss of bands) due to the presence of starch and further decrease upon H addition. Enhancement of IR bands at 430–552 (Zn-O vibrations) and 1500–1640 cm$^{-1}$ (Zn-O stretching) for the corresponding ZnO:H samples was also observed.

## Competing Interests

The authors declare that there are no competing interests regarding the publication of this article.

## Acknowledgments

The authors wish to acknowledge the Centre of Nanotechnology and Advanced Materials, Engineering Development Institute (EMDI), Akure, Ondo State, for the X-ray diffraction facility used and also the Materials Laboratory of Kwara State University, Illorin, for their SEM and EDX facilities. They would also like to thank Mr. F. Chioma of the University of Ibadan for the FT-IR analysis and Tetfund, Nigeria, for conference sponsorship.

## References


[1] P. W. Atkins, T. Overtone, J. Rourke, M. Weller, and F. Armstrong, *Inorganic Chemistry*, Oxford University Press, Oxford, UK, 5th edition, 2010.

[2] A. S. Shaporev, V. K. Ivanov, A. E. Baranchikov, O. S. Polezhaeva, and Y. D. Tret'yakov, "ZnO formation under hydrothermal conditions from zinc hydroxide compounds with various chemical histories," *Russian Journal of Inorganic Chemistry*, vol. 52, no. 12, pp. 1811–1816, 2007.

[3] H. Kumar and R. Rani, "Structural and optical characterization of ZnO nanoparticles synthesized by microemulsion route," *International Letters of Chemistry, Physics and Astronomy*, vol. 19, pp. 26–36, 2013.

[4] R. A. McBride, J. M. Kelly, and D. E. McCormack, "Growth of well-defined ZnO microparticles by hydroxide ion hydrolysis of zinc salts," *Journal of Materials Chemistry*, vol. 13, no. 5, pp. 1196–1201, 2003.

[5] C. G. Van de Walle, "Hydrogen as a cause of doping in zinc oxide," *Physical Review Letters*, vol. 85, no. 5, pp. 1012–1015, 2000.

[6] A. Janotti and C. G. Van De Walle, "Hydrogen multicentre bonds," *Nature Materials*, vol. 6, no. 1, pp. 44–47, 2007.

[7] E. V. Lavrov, "Hydrogen in ZnO: an infra-red absorption study," *Defect and Diffusion Forum*, vol. 226–228, no. 1, pp. 181–189, 2004.

[8] C. G. Van de Walle, "Hydrogen interactions with semiconductors and oxides," in *Proceedings of the 1st International Workshop on Hydrogen in Materials and Vacuum Systems*, G. R. Myneni and Chattopadhyay, Eds., vol. 671 of *AIP Conference Proceedings*, pp. 33–39, 2003.

[9] A. Abliz, C.-W. Huang, J. Wang et al., "Rational design of ZnO:H/ZnO bilayer structure for high-performance thin-film transistors," *ACS Applied Materials and Interfaces*, vol. 8, no. 12, pp. 7862–7868, 2016.

[10] K. Ghule, A. V. Ghule, B.-J. Chen, and Y.-C. Ling, "Preparation and characterization of ZnO nanoparticles coated paper and its antibacterial activity study," *Green Chemistry*, vol. 8, no. 12, pp. 1034–1041, 2006.

[11] "Hydrothermal synthesis of hydrated zinc oxide nanoparticles and its characterization," *Chemical Science Transactions*, vol. 2, no. S1, pp. S33–S36, 2013.

[12] Y. Dimitriev, M. Gancheva, and R. Iordanova, "Synthesis of zno by mechanochemical decomposition of zinc carbonate hydroxide," *Journal of the University of Chemical Technology and Metallurgy*, vol. 46, no. 3, pp. 243–248, 2011.

[13] F. Ahmed, S. Kumar, N. Arshi, M. S. Anwar, and R. Prakash, "Growth and characterization of ZnO nanorods by microwave-assisted route: Green chemistry approach," *Advanced Materials Letters*, vol. 2, no. 3, pp. 183–187, 2011.

[14] K. Nejati, Z. Rezvani, and R. Pakizevand, "Synthesis of ZnO nanoparticles and investigation of the ionic template effect on their size and shape," *International Nano Letters*, vol. 1, pp. 75–81, 2011.

[15] A. Khorsand Zak, R. Razali, W. H. Abd Majid, and M. Darroudi, "Synthesis and characterization of a narrow size distribution of zinc oxide nanoparticles," *International Journal of Nanomedicine*, vol. 6, no. 1, pp. 1399–1403, 2011.

[16] J. F. Muth, R. M. Kolbas, A. K. Sharma, S. Oktyabrsky, and J. Narayan, "Excitonic structure and absorption coefficient measurements of ZnO single crystal epitaxial films deposited by pulsed laser deposition," *Journal of Applied Physics*, vol. 85, no. 11, pp. 7884–7887, 1999.

[17] H. J. Chang, C. Z. Lu, Y. Wang et al., "Optical properties of ZnO nanocrystals synthesized by using sol-gel method," *Journal of the Korean Physical Society*, vol. 45, no. 4, pp. 959–962, 2004.

[18] S. Dutta and B. N. Ganguly, "Characterization of ZnO nanoparticles grown in presence of Folic acid template," *Journal of Nanobiotechnology*, vol. 10, article 29, 2012.

[19] S. Anita, T. Ramachandran, R. Rajendran, C. V. Koushik, and M. Mahalakshmi, "Preparation and characterization of zinc oxide nanoparticles and a study of the anti-microbial property of cotton fabric treated with the particles," *Journal of Textile and Apparel, Technology and Management*, vol. 6, no. 4, 2010.

[20] C. G. Van de Walle, "Hydrogen in materials and vacuum systems," in *Proceedings of the 1st International Workshop on Hydrogen in Materials and Vacuum Systems*, G. R. Myneni and S. Chattopadhyay, Eds., vol. 671 of *AIP Conference Proceedings*, pp. 33–39, Newport News, Va, USA, November 2002.

[21] W. M. Hlaing Oo and M. D. McCluskey, "Infrared spectroscopy of impurities in ZnO nanoparticles," *MRS Proceedings*, vol. 864, E4.40, 2005.

[22] S. J. Jokela, M. D. McCluskey, and K. G. Lynn, "Infrared spectroscopy of hydrogen in annealed zinc oxide," *Physica B: Condensed Matter*, vol. 340-342, pp. 221–224, 2003.

[23] Z. Zhang, D. C. Look, R. Schifano, K. M. Johansen, B. G. Svensson, and L. J. Brillson, "Process dependence of H passivation and doping in H-implanted ZnO," *Journal of Physics D: Applied Physics*, vol. 46, no. 5, Article ID 055107, 2013.

[24] H. E. Swanson and R. K. Fuyat, "Standard X-ray diffraction powder patterns," *National Bureau of Standards (U.S.), Monograph 25, Circular 539*, vol. 1, 1953.

[25] B. Fultz and J. M. Howe, *Transmission Electron Microscopy and Diffraction of Materials (Graduate Texts in Physics)*, Springer, Berlin, Germany, 4th edition, 2013.

[26] J. L. Konne and K. Okpara, "Remediation of nickel from crude oil obtained from bomu oil field using cassava waste water starch stabilized magnetic nanoparticles," *Energy and Environment Research*, vol. 4, no. 1, pp. 25–31, 2014.